ISSN 1063-7826, Semiconductors, 2020, Vol. 54, No. 11, pp. 1398–1405. © Pleiades Publishing, Ltd., 2020.

SPECTROSCOPY, INTERACTION WITH RADIATION

Optimal Estimation of Schottky Diode Parameters Using Advanced Swarm Intelligence Algorithms

A. Rabehi[a,b,*], B. Nail[b], H. Helal[a], A. Douara[b], A. Ziane[a], M. Amrani[a], B. Akkal[a], and Z. Benamara[a]

[a] *Laboratoire de Micro-électronique Appliquée, Université Djillali Liabés de Sidi Bel Abbés, BP 89, Sidi Bel Abbés, 22000 Algeria*

[b] *Institute of Science and Technology, Tissemsilt University Center, Tissemsilt, 38000 Algeria*

**e-mail: rab_ehi@hotmail.fr*

Received May 11, 2020; revised May 11, 2020; accepted July 6, 2020

Abstract—This work deals with estimation of the Schottky diode (Au|GaN|GaAs) optimal parameters. For this purpose, advanced swarm intelligence (SI) algorithms have been applied, i.e., Harris hawks optimization, ant lion optimizer (ALO), grey wolf optimizer, and whale optimization algorithm. The performance of the SI algorithms has been investigated by a comparative study following the analytical methods developed by Kaminski I, Cheung and Cheung, Norde, and Mikhelashvili. The comparative results show that the ALO algorithm gives minimum RMSE criteria, with best parameters estimation against all the SI optimizers and the analytical techniques.

Keywords: Schottky diodes, Au, GaN, GaAs, swarm intelligence algorithms, parameters estimation, barrier height

DOI: 10.1134/S1063782620110214

1. INTRODUCTION

Fabrication and characterization of metal-semiconductor Schottky contacts have attracted much attention in recent years [1–5]. This is due to the potential application in various electronic and optoelectronic devices, such as high-frequency field-effect transistors (FETs), microwave FETs, RF detectors, photodiodes, laser diodes, and solar cells [3]. It is well known that for ideal Schottky contacts, the dominant current is the thermionic emission (TE) [5–9]. But in practice, this mechanism deviates due to the effect of tunnel currents such as thermionic field emission (TFE) and field emission (FE) mechanisms [10]. A non-dimensional parameter called the ideality factor n, as well as the series resistance are included in the model of the current–voltage $I(V)$ characteristics to take into account non-ideal Schottky contacts behavior [7, 11]. Accurate knowledge of the electrical parameters is of importance for the quality control and the evaluation of the Schottky device's performance. Several methods have been proposed to extract the electrical parameters such as ideality factor n, barrier height ϕ_{bn}, and series resistance R_S from the $I(V)$ characteristics for non-ideal Schottky contacts [7, 12–15]. However, most of these methods lack credibility and reliability. They are essentially based on identifying each parameter from restricted regions of the $I(V)$ characteristics, while the effect of other parameters is assumed to be negligible [9].

Evolutionary algorithm (EA) techniques based on artificial intelligence are effective methods in semiconductor device modeling. EA such as genetic algorithm, the penalty-based differential evolution, the particle swarm optimization, and the teaching-learning-based optimization are stochastic optimization methods that appear to be very efficient in optimizing real-valued multi-modal objective functions. In contrast to numerical methods, EA can handle non-linear functions without requiring derivative information and depends weakly on the starting values of the parameters that are introduced prior to algorithm running [16]. EA is considered to be more promising than other computational methods [17].

In the present study, we consider new evolutionary algorithms—ant lion optimizer (ALO), grey wolf optimizer (GWO), Harris hawks optimization (HHO), and whale optimization algorithm (WOA)—of Schottky barrier diode (SBD) parameters extraction, and we compared them to other already existing analytical techniques.

2. EXPERIMENTAL PROCEDURES

Si-doped n-GaAs wafers were used in this study, with thickness of 400 μm, (100) orientation and doping concentration of $N_d = 4.9 \times 10^{15}$ cm^{-3}. The wafers were cleaned in sulfuric acid (H_2SO_4), deionized water

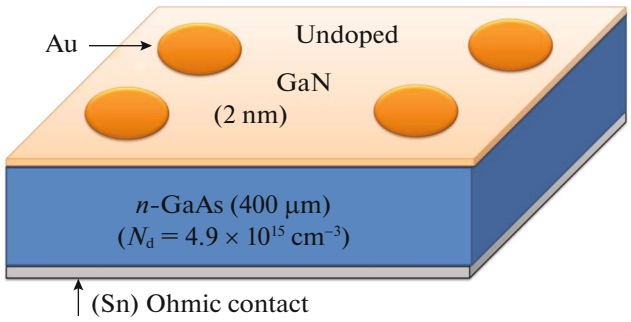

Fig. 1. The elaborated structure of Au|2 nm-GaN|*n*-GaAs Schottky diodes.

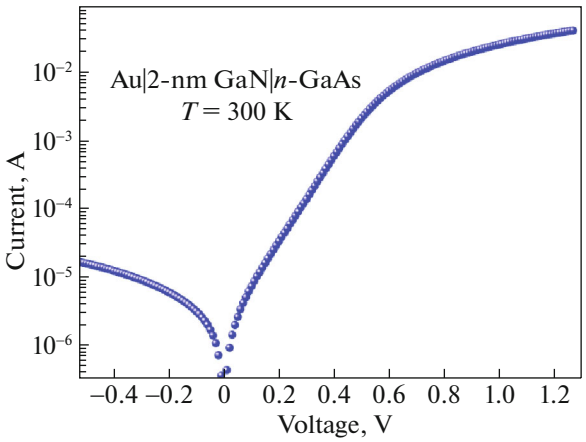

Fig. 2. Current–voltage characteristic of Au|GaN|GaAs diode.

(H_2O), cold methanol (CH_3OH), and hot methanol (CH_3OH), and dried by nitrogen gas (N_2), sequentially. Then, the *n*-GaAs wafers were bombarded using the ionic bombardment Ar^+ source, with 1 keV ion energy and 5 μA cm^{-2} sample current in ultra-high-vacuum (UHV) chamber.

The wafers were nitrated to obtain 2 nm of GaN layer, using glow discharge source after heating at 500°C for 1 h. The non-doped GaN layer was growing under nitrogen flow, with power of 5 W of, for 30 min at 500°C of temperature, in UHV chamber. After the nitration process, the structures were annealed at 620°C for 60 min, in order to restructure and reorganize the growing GaN layer. Finally, Au Schottky contacts of 0.6-mm diameter and 0.1 μm of thickness were performed using the Knudsen evaporator. The Sn ohmic contacts were evaporated on back side of the *n*-GaAs wafer, at a temperature of 350°C for 5 min. The elaborated structure Au|2nm-GaN|*n*-GaAs is illustrated in Fig. 1.

The current–voltage measurements $I(V)$ of the Schottky structures (Fig. 2) were investigated in the dark and at room temperature, using an HP Semiconductor Parameters Analyzer 4155B.

Table 1. Electrical parameters obtained from $I(V)$ curves of Au|GaN|*n*-GaAs Schottky diode using analytical techniques

Method of calculation	n	R_S, Ω	ϕ_{bn}, eV	RMSE
Norde	—	22.63	0.69	—
Kaminski II	1.90	15.63	—	—
Cheung and Cheung	1.92	16.22	0.62	6.7033×10^{-7}
Mikhelashvili	1.98	14.04	0.58	8.1556×10^{-5}

3. THE DESCRIPTION OF THE SBD MODEL

For the ideal SBD, it is assumed that the forward bias current of the device is due to the thermionic emission current and can be expressed as [18]

$$I = I_0\left[\exp\left(\frac{q(V - IR_s)}{nKT}\right) - 1\right], \quad (1)$$

where

$$I_0 = AA^*T^2\exp\left(-\frac{q\phi_{bn}}{kT}\right) \quad (2)$$

is the saturation current. In the above equations, the symbols of V, I, A, A^*, q, T, k are the bias voltage, diode current, diode area, Richardson constant, the electron charge, absolute temperature, and the Boltzmann constant, respectively. The ideality factor n, Schottky barrier height ϕ_{bn}, and series resistance R_S are the characteristic parameters of the SBDs and should be determined as accurately as possible from experimental $I(V)$ characteristics.

4. PARAMETER EXTRACTION METHODS

4.1. Analytical Methods

4.1.1. Cheung and Cheung method. The values of R_S and n can be determined from the following functions [7, 19]:

$$G(I) = \frac{\partial V}{\partial(\ln I)} = \frac{nkT}{q} + IR_S. \quad (3)$$

The linear fitting permits to estimate R_S and n.

To obtain barrier height, Cheung and Cheung defined a function as [14, 20]:

$$H(I) = V - \left(\frac{nkT}{q}\right)\ln\left(\frac{I}{AA^*T^2}\right) = n\phi_{bn} + IR_S. \quad (4)$$

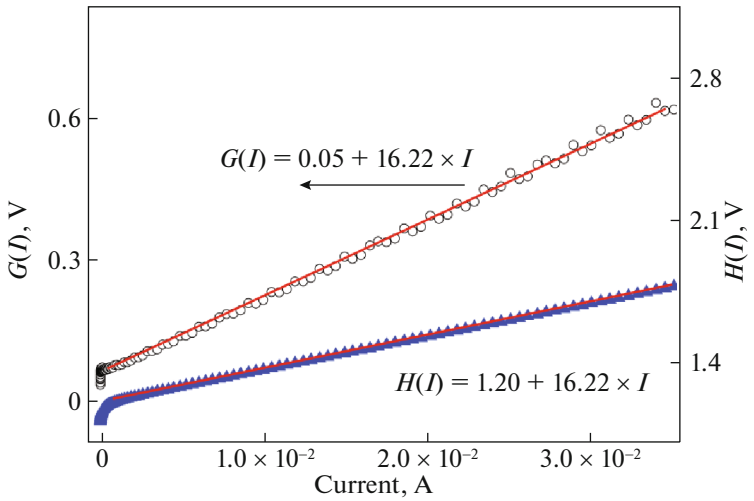

Fig. 3. Illustration of the functions G and H.

A plot of $H(I)$ also yields a straight line, with a y-axis intercept that equals to $n\phi_{bn}$. The plots of $G(I)$ and $H(I)$ are shown in Fig. 3, and the obtained values of the parameters are shown in Table 1.

4.1.2. Kaminski II method. This method [16, 21] based on the plot of Y vs. X, where

$$Y_k = \frac{\ln(I_j/I_i)}{I_j - I_i} \text{ and } X_k = \frac{V_j - V_i}{I_j - I_i}, \quad (5)$$

$$i \in (1,\ldots,N_p - 1), \quad j \in (i+1,\ldots,N_p),$$
$$k \in (1,\ldots,N_p(N_p - 1)/2),$$

where N_p is the number of $I(V)$ data samples.

The plot of Y vs. X is expected to be linear [16]:

$$Y = q(-R_S + X)/nkT, \quad (6)$$

and the linear fitting permits to estimate R_S and n. The values obtained using the Kaminski method are shown in Table 1 above.

The most interesting point with this method is the fact that we do not have any limitation conditions on the voltage hop and it is very easy to use.

4.1.3. Norde method. The function of Norde [12, 22] is defined as follows:

$$F(V) = \frac{V}{\gamma} - \frac{kT}{q}\ln\left(\frac{I(V)}{AA^*T^2}\right), \quad (7)$$

where γ is the first integer greater than the ideality factor, $I(V)$ is current obtained from the $I(V)$ curve. When the minimum of the $F(V)$ plot is determined, the Schottky barrier height can be found using

$$\phi_{bn} = F(V_0) + \frac{V_0}{\gamma} - \frac{kT}{q}, \quad (8)$$

where $F(V_0)$ is the minimum point of $F(V)$, and V_0 is the minimum voltage of the $F(V)$ plot [3]. Figure 4 depicts the $F(V)$ plot of the structure. The values obtained using the Norde method are shown in Table 1.

4.1.4. Mikhelashvili method. One of the techniques suggested by Mikhelashvili et al. [23] starts from the function $\alpha(V)$:

$$\alpha(V) = \frac{\partial(\ln I)}{\partial(\ln V)}. \quad (9)$$

The parameters value deduced by

$$R_S = \frac{V_{max}}{\alpha_{max}^2 I_{max}}, \quad (10)$$

$$n = \frac{qV_{max}(\alpha_{max} - 1)}{\alpha_{max}^2 kT}, \quad (11)$$

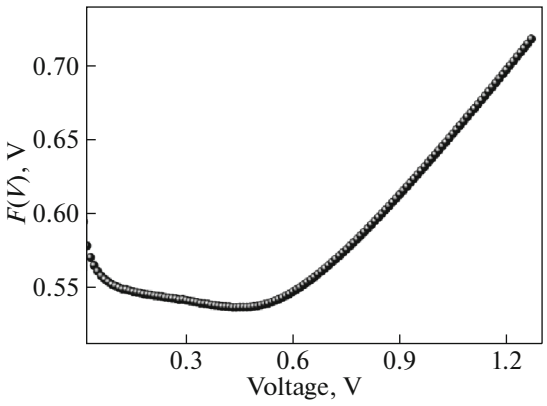

Fig. 4. The $F(V)$ plot of Au|GaN|n-GaAs Schottky diode.

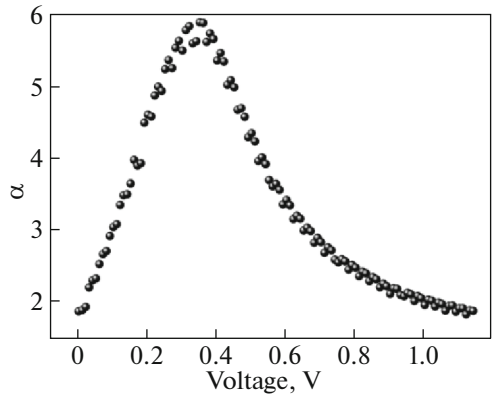

Fig. 5. The Mikhelashvili's curve.

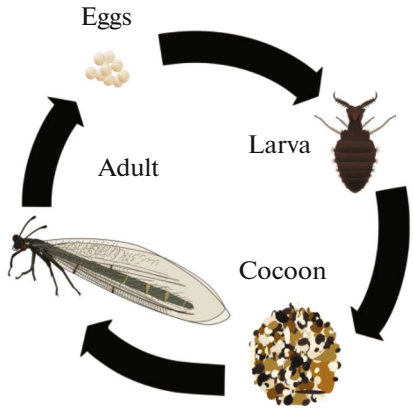

Fig. 6. Ant lion life cycle.

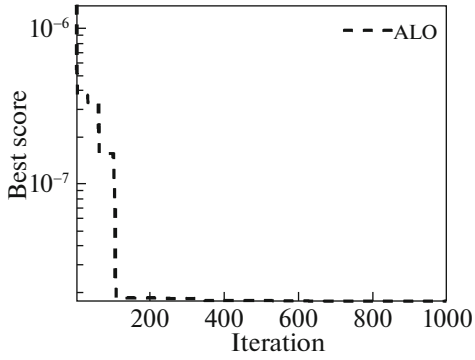

Fig. 7. The objective function in terms of ALO iterations.

$$\phi_{bn} = \frac{kT}{q}\left[\alpha_{\max} + 1 - \ln\left(\frac{I_{\max}}{AA^{*}T^{2}}\right)\right], \qquad (12)$$

where α_{max} and V_{max} are the coordinates of maximum point in the plot α vs. V (see Fig. 5); I_{max} is the current value at the voltage V_{max}. The obtained values of the parameters are shown in Table 1.

4.2. Evolutionary Algorithms

In order to estimate the current of Schottky diode with evolutionary algorithms, the following function has been chosen to minimize the root mean square error (RMSE) as follows:

$$J = \min_x \sqrt{\frac{\Sigma_i^N e_i^2}{N}}, \qquad (13)$$

where $e_i = I_i - \hat{I}_i$ is the error between the estimated and the real measurement, N is the number of the experimental data, x is the optimization vector containing the parameters of Schottky diode.

After maximal iteration equal to 1000, and the searching range for each parameter is set as follows: $\phi_{bn} \in [0; 1]$, $n \in [1, 2]$, $R_S \in [0; 100]$.

4.2.1. Ant lion optimizer. ALO is a new successful population-based meta-heuristic algorithm (MHA) that tries to mimic the idealized hunting activities of ant lions in the nature [24]. The name of this insect originates from its exceptional hunting tactics and specifies its beloved quarry. They dig a cone-shaped pit-trap in the sand using certain circular motions with their powerful jaw. After building a cone-shaped trap, these sit-and-wait hunters will hide themselves at the bottom of the cone and wait for often ants to be tripping over their trap with steep shores. After detecting that an insect cannot escape the cone-shaped pit, they attack to kill the prey. As in the nature, the insects attempt to survive from the faced traps, they will perform some abrupt movements to get away from predator. At this stage, ant lions intelligently start to toss sand-grains just before the edges of the pit to make the frightened victim slide into the deepest point of the pit. When a quarry cannot keep its safe distance to the jaw, it will be dragged under the surface and killed. Extra thought-provoking behavior performed by these hunters is the proportion of the dimensions of the pit affected with two factors: degree of malnutrition and phase of the moon. Referring to the above behaviors and tricks, the ALO has two classes of search agents, namely, ant and ant lions. The best search agents are selected as ant lions that never change their positions except for the situation they substitute a particular ant. Ant agents can carry out random walks in the solution space and may be captured by an ant lion if being trapped in a pit [25].

Figure 6 shows the life-cycle behavior of ant lion in the nature, on which the idea for ALO algorithm was inspired.

Figures 7 and 8 show the optimization evolution in each iteration of ALO.

4.2.2. Grey wolf optimizer. GWO is a new MHA that belongs to the swarm intelligence (SI) category. This algorithm is inspired by the hunting process

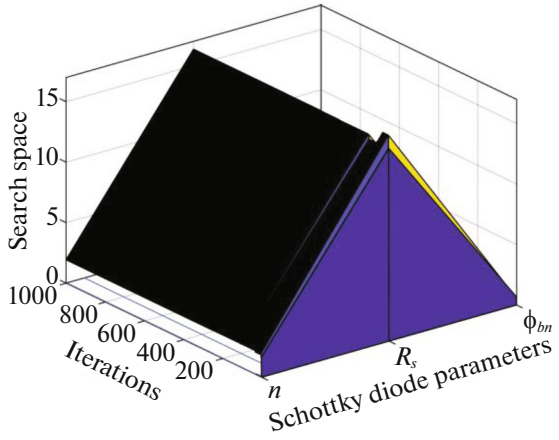

Fig. 8. Schottky diode parameters tuning based on ALO.

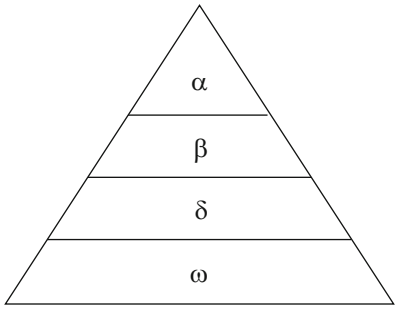

Fig. 9. Leadership hierarchy of grey wolves.

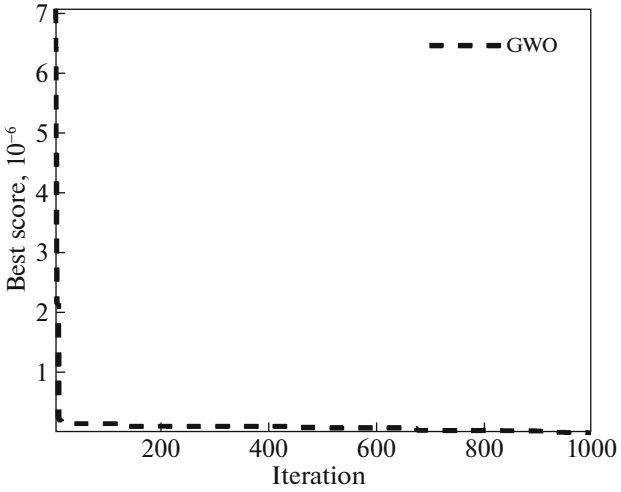

Fig. 10. The objective function in terms of GWO iterations.

found in grey wolves. This is unique as it follows the leadership hierarchy of the grey wolves. Grey wolves are well known for pack hunting and no other SI methods were proposed to follow this hierarchical hunting behavior.

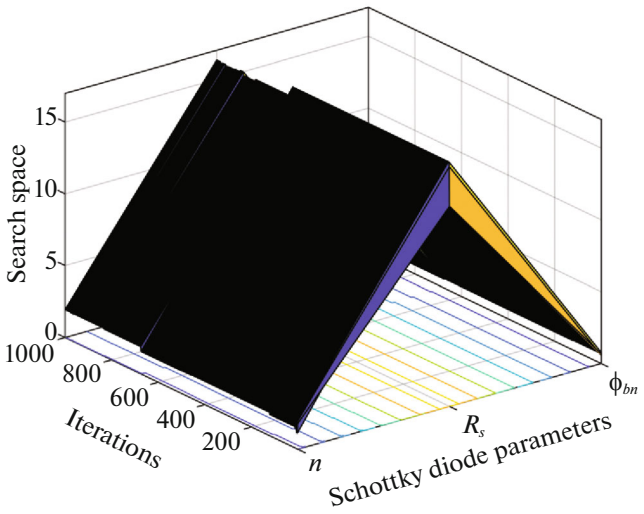

Fig. 11. Schottky diode parameters tuning based on GWO.

Grey wolf belongs to Canidae family. They prefer to live in a group, generally called a pack. The group consists of 12–15 members on an average. They follow a strict social dominant hierarchy. The leader wolves are represented by alpha. Alpha wolves constitute a male and a female wolf. They have the authority to decide the resting place, time of hunting, etc., for the whole group. They may not be the strongest ones, but are the best ones to manage the group. The orders of the leader wolves are followed by the pack. The betas are next in rank to the alphas and assist the leader in taking decision. The beta is an advisor to alpha and discipline for the group. They are the best wolves next to be the alpha to take their position in the case of death or retirement of an alpha wolf. Omega wolves are the lowest in rank. They have to follow the orders of all other dominant wolves and allowed to eat last. If a wolf does not belong to any of the above categories, then it is called delta. Delta wolves dominate omegas and follow the orders of alphas and betas (Fig. 9) [26, 27].

Figures 10 and 11 show the optimization evolution in each iteration of GWO.

4.2.3. Harris hawks optimizer. HHO is a novel optimization method developed by Heidari et al. [28]. HHO is a nature-inspired optimization algorithm inspired by the Harris hawk birds' behavior modeling. The essence of the algorithm is the cooperation between hawks in hunting the prey. Based on this algorithm, a group of Harris hawks attacks the prey from different directions to take it by surprise. Evidently, the prey's escape pattern is proportional to the Harris hawks chase model.

Birds cooperate in the process of attack. Meanwhile, the leader of the Harris hawks attacks the target prey, follows it, and suddenly moves out of sight, and

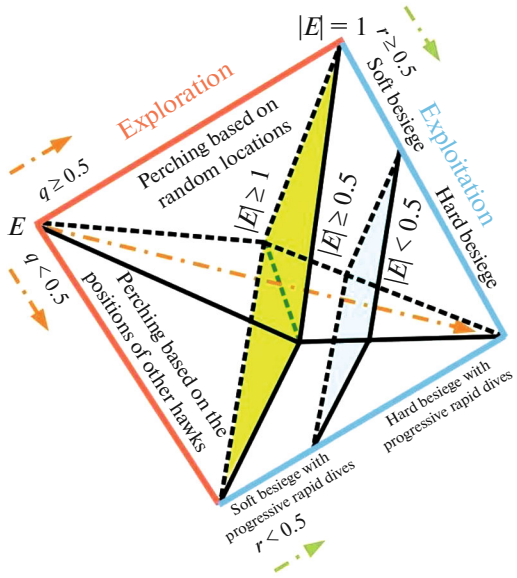

Fig. 12. Different phases of HHO algorithm.

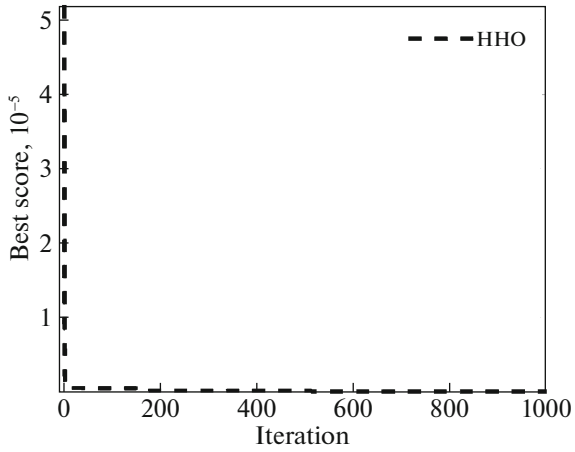

Fig. 13. The objective function in terms of HHO iterations.

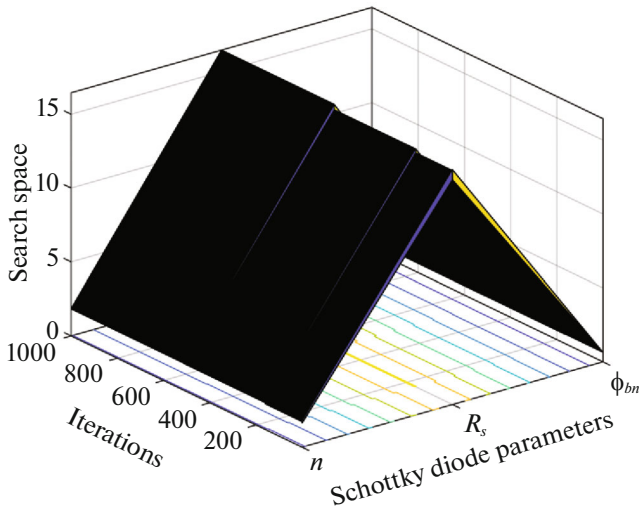

Fig. 14. Schottky diode parameters tuning based on HHO.

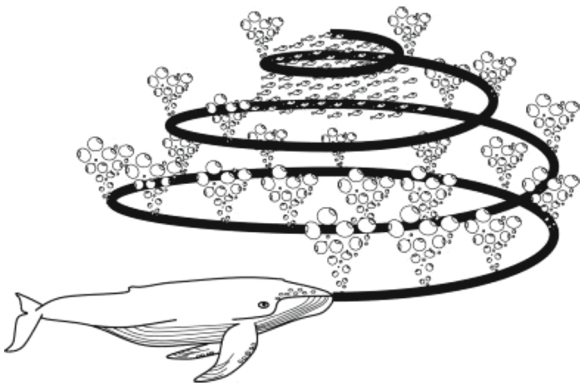

Fig. 15. Bubble-net feeding behavior of humpback whales.

the next Harris hawk continues the chase. This strategy tires the prey and eventually results in its capture. HHO algorithm is more superior to other algorithms on its applicability to constrain problems. Moreover, HHO, which is a global optimizer, can maintain its balance between exploitation and exploration phases. The HHO algorithm has three phases. The first phase is the ability of exploration [29], as shown in Fig. 12.

Figures 13 and 14 show the optimization evolution in each iteration of HHO.

4.2.4. Whale optimization algorithm. WOA was proposed by Mirjalili and Lewis for optimizing numerical problems [30]. The algorithm simulates the intelligence and hunting behavior of humpback whales. This foraging behavior is called bubble-net feeding method that is only be observed in humpback whales. The whales create the typical bubbles along a circle path while encircling prey during hunting. Simply, bubble-net hunting behavior could describe such that humpback whales dive down approximation 12 m and then create the bubble in a spiral shape around the prey and then swim upward the surface following the bubbles in order to perform optimization [31], as shown in Fig. 15.

Figures 16 and 17 show the optimization evolution in each iteration of WOA.

5. RESULTS AND DISCUSSION

Table 2 lists the extracted values of ideality factor n, series resistance R_S, and barrier height ϕ_{bn} obtained by the four methods.

The value of ideality factor n is found to vary from 1.83 to 1.98 in different methods, which shows non-ideal $I(V)$ behaviour. The value of barrier height ϕ_{bn} is found to vary from 0.609 to 0.622 eV from Cheung's functions and the SI algorithms; this result is similar to that obtained by Ambrico et al. [32].

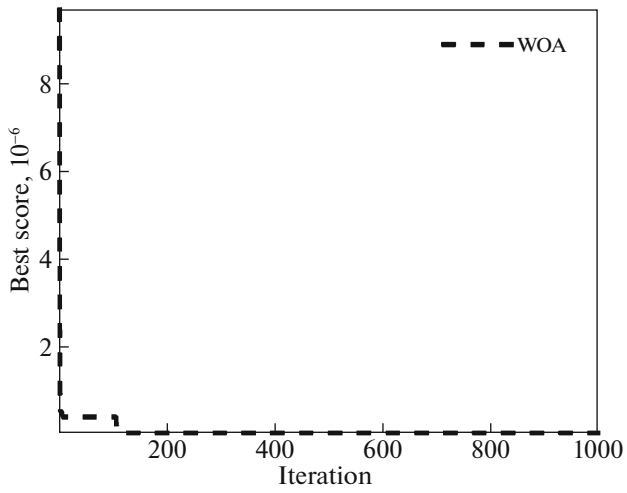

Fig. 16. The objective function in terms of WOA iterations.

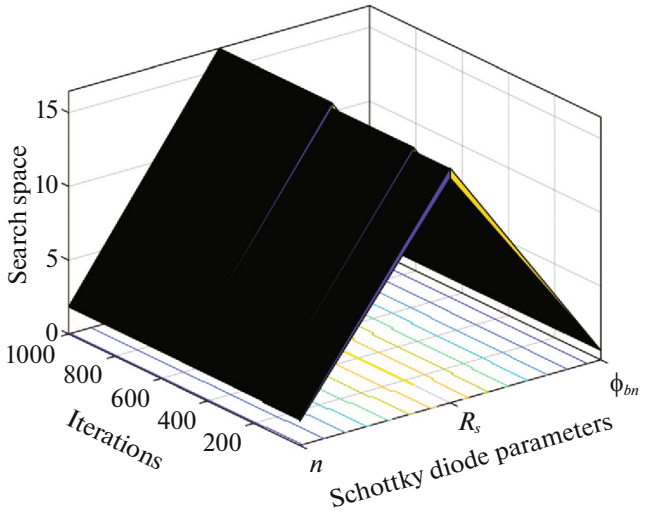

Fig. 17. Schottky diode parameters tuning based on WOA.

The ϕ_{bn} and R_S values obtained by Norde and Mikhelashvili methods are systematically different than those obtained by Cheung's method. These differences may be attributed to the extraction of information from different regions of the forward-bias current-voltage plot [33], and perhaps because Norde's functions are performed for the whole forward-bias region of the $I(V)$ curve. In contrast, Cheung's functions are only executed for the non-linear part of the forward-bias $I(V)$ curve.

The series resistance obtained from the Cheung's method is in close agreement with the value obtained from the evolutionary algorithms. This case shows the consistency of Cheung's approach.

It can be observed from Table 2 that the SI algorithms do not particularly call for initial guesses as close as possible to the solution in the parameter estimation of the Schottky barrier diode, while only requiring a broader search range specified for each parameter.

Furthermore, the validation criteria provide by RMSE between the real and the estimated parameters of the studied SI algorithms: HHO, ALO, GWO, and WOA are 2.8658×10^{-8}, 1.7622×10^{-8}, 1.8096×10^{-8}, and 3.5739×10^{-8}, respectively, which indicates that the optimum searching quality of the ALO method has given the best estimation parameters.

Table 2. Electrical parameters obtained from $I(V)$ curves of Au|GaN|n-GaAs Schottky diode using SI algorithms

Method of calculation	n	R_S, Ω	ϕ_{bn}, eV	RMSE
HHO	1.83755	16.4519	0.622877	2.8658×10^{-8}
ALO	1.92967	16.3555	0.609397	1.7622×10^{-8}
GWO	1.95000	16.3311	0.606593	1.8096×10^{-8}
WOA	1.89653	16.2453	0.616768	3.5739×10^{-8}

Table 3. SI algorithms parameters

Parameters	Values
Lower bound [n, R_S, ϕ_{bn}]	[1, 10, 0.4]
Upper bound [n, R_S, ϕ_{bn}]	[1.95, 17, 0.8]
Dimension	3
Number of iteration	500
Number of particles	20

The SI algorithms HHO, ALO, GWO, and WOA were applied under the same parameters setting, as it' s presented in the Table 3.

CONCLUSIONS

In this paper, by using the Au|GaN|GaAs SBD as an example, we have presented techniques to improve the identified electrical parameters accuracy of the devices, using SI algorithms (HHO, ALO, GWO, and WOA). It is based on formulating the parameter identification problem as a search-and-optimization one.

Compared with the analytical techniques methods, the proposed SI algorithms have superior performance, according to estimation accuracy and computational efficiency. In consideration of evolutionary algorithms, the ALO method is favorable over the HHO, the GWO, and the WOA due to the minimal RMSE.

This study, test, and comparative analysis of analytical techniques and SI algorithms for determination of Schottky diode parameters should be useful for further research and development on metal–semiconductor devices.

CONFLICT OF INTEREST

The authors declare that they have no conflict of interest.

REFERENCES

1. H. Helal, Z. Benamara, A. H. Kacha, M. Amrani, A. Rabehi, B. Akkal, G. Monier, and C. Robert-Goumet, Superlatt. Microstruct. **135**, 106276 (2019).
2. H. Helal, Z. Benamara, M. B. Arbia, A. Khettou, A. Rabehi, A. H. Kacha, and M. Amrani, Int. J. Numer. Model.: Electron. Networks. Dev. Fields **33**, e2714 (2020).
3. A. Rabehi, M. Amrani, Z. Benamara, B. Akkal, A. Hatem-Kacha, C. Robert-Goumet, G. Monier, and B. Gruzza, Eur. Phys. J. Appl. Phys. **72**, 10102 (2015).
4. A. Rabehi, M. Amrani, Z. Benamara, B. Akkal, and A. Kacha, Optik **127**, 6412 (2016).
5. A. Kacha, B. Akkal, Z. Benamara, C. Robert-Goumet, G. Monier, and B. Gruzza, Mol. Cryst. Liq. Cryst. **627**, 66 (2016).
6. B. Akkal, Z. Benamara, N. B. Bouiadjra, S. Tizi, and B. Gruzza, Appl. Surf. Sci. **253**, 1065 (2006).
7. S. Cheung and N. Cheung, Appl. Phys. Lett. **49**, 85 (1986).
8. M. A. Ebeoglu, Phys. B (Amsterdam, Neth.) **403**, 61 (2008).
9. E. Rhoderick and R. Williams, *Metal–Semiconductor Contacts* (Clarendon, Oxford, 1988).
10. E. Özavcï, S. Demirezen, U. Aydemir, and Ş. Altındal, Sens. Actuators, A **194**, 259 (2013).
11. S. M. Sze and K. K. Ng, *Physics of Semiconductor Devices* (Wiley, Chichester, 2006).
12. H. Norde, J. Appl. Phys. **50**, 5052 (1979).
13. K. Sato and Y. Yasumura, J. Appl. Phys. **58**, 3655 (1985).
14. J. H. Werner, Appl. Phys. A **47**, 291 (1988).
15. R. M. Cibils and R. H. Buitrago, J. Appl. Phys. **58**, 1075 (1985).
16. O. Y. Olikh, J. Appl. Phys. **118**, 024502 (2015).
17. K. Ishaque, Z. Salam, H. Taheri, and A. Shamsudin, Solar Energy **85**, 1768 (2011).
18. R. Padma and V. R. Reddy, Semiconductors **51**, 1641 (2017).
19. N. Kononov and S. Dorofeev, Semiconductors **51**, 608 (2017).
20. A. Rabehi, M. Amrani, Z. Benamara, B. Akkal, A. Ziane, M. Guermoui, A. Hatem-Kacha, G. Monier, B. Gruzza, and L. Bideux, Semiconductors **52**, 1998 (2018).
21. A. Kaminski, J. Marchand, and A. Laugier, Solid-State Electron. **43**, 741 (1999).
22. S. Kumar, M. Kumar, and S. Krishnaveni, Semiconductors **54**, 169 (2020).
23. V. Mikhelashvili, G. Eisenstein, V. Garber, S. Fainleib, G. Bahir, D. Ritter, M. Orenstein, and A. Peer, J. Appl. Phys. **85**, 6873 (1999).
24. S. Mirjalili, Adv. Eng. Software **83**, 80 (2015).
25. A. A. Heidari, H. Faris, S. Mirjalili, I. Aljarah, and M. Mafarja, *Nature-Inspired Optimizers*, Vol. 811 of *Studies in Computational Intelligence* (Springer, Berlin, 2020), p. 23.
26. S. Mirjalili, S. M. Mirjalili, and A. Lewis, Adv. Eng. Software **69**, 46 (2014).
27. M. Panda and B. Das, in *Proceedings of the 3rd International Conference on Microelectronics, Computing and Communication Systems* (2019), p. 179.
28. A. A. Heidari, S. Mirjalili, H. Faris, I. Aljarah, M. Mafarja, and H. Chen, Future Gener. Comput. Syst. **97**, 849 (2019).
29. A. Abbasi, B. Firouzi, and P. Sendur, Eng. Comput., 1 (2019).
30. S. Mirjalili and A. Lewis, Adv. Eng. Software **95**, 51 (2016).
31. J. Nasiri and F. M. Khiyabani, Cogent Math. Stat. **5**, 1483565 (2018).
32. W. Gao, P. R. Berger, R. G. Hunsperger, G. Zydzik, W. Rhodes, H. O'Bryan, D. Sivco, and A. Cho, Appl. Phys. Lett. **66**, 3471 (1995).
33. Ş. Karataş, N. Yildirim, and A. Türüt, Superlatt. Microstruct. **64**, 483 (2013).